**MARE PROTOLITH PROPERTIES AND SECONDARY IMPACTS INFERRED FROM ROCKY CRATER POPULATIONS.** M. A. Chertok[1], P. G. Lucey[1], E. S. Costello[1], S. M. Ireland[2], [1]University of Hawai'i at Mānoa (mchertok@hawaii.edu), [2]Jet Propulsion Laboratory.

**Introduction:** Impactors of sufficient size and energy that strike the lunar surface can excavate coherent rocks buried beneath thin mare regolith (3-5 m) [1]. The excavation of rocks may vary by the type of collision and the character of the substrate, where the nature of buried mare lava flows ("protolith") [2] may limit the abundance of rocks ejected by an impact. The initial collision of a meteorite forms primary craters, whereas secondary craters are formed by material expelled by the primary impact. Because secondary impacts are less energetic than primary impacts [3], it stands to reason that these projectiles may not be capable of breaking up and ejecting rocks to the same capacity as a primary impact.

Size-frequency distributions (SFDs) are sensitive to differences in crater populations and may indicate variations in substrate and impactor velocity. Therefore, by inspecting the SFDs of craters with rocks in their ejecta, we may gain insight into controls on rock excavation including the effects of both substrate and secondary inclusions.

**Site Selection:** This study features counts of rocky craters at 15 lunar mare sites. These sites (denoted as name and unit number (e.g., Humorum 6) [4, 5, 6]) overlap with areas counted by Hiesinger et al. for surface age estimation [4, 5, 6] but are larger to collect adequate statistics on rocky craters that are less abundant than the total population. Counted areas range in size from 3,200-3,700 km$^2$. Sites include seven locations within Oceanus Procellarum, two in Mare Imbrium, two in Mare Nubium, one in Mare Serenitatis, one in Mare Humorum, and two in Mare Tranquillitatis.

**Data:** We use shaded relief imagery generated from the merged LOLA/Terrain camera DEM data set for the crater counting [7] and rock abundance or "rockiness" is quantified using thermal inertia data from LRO Diviner following Bandfield et al., 2011 [8]. From the rock abundance parameter, we can then determine how crater size-frequency distributions vary with degree of rockiness.

**Methods:** The CraterTools plug-in for ArcMap [9] was used to count craters, all of which are larger than 200 m in diameter to ensure penetration to bedrock [10]; however, the portion of the dataset for which we focus includes craters with diameters greater than 600 m to ensure accurate counts [11]. Secondary impact craters were included in the crater counts to capture the entirety of the crater population. CraterPy [12] was also used to extract rock abundance statistics from the crater ejecta, which is defined from 1.1 to 2 crater radii.

SFDs were computed [13, 14] for the total crater populations as well as cumulative ejecta rockiness bins. The bins are defined by 1% increments of rock abundance. Each SFD is plotted as cumulative rock abundance, e.g., ≥1% rock abundance. We parameterized each rock abundance binned SFD using the slope of the distribution to compare the rock abundance variation among the study areas.

**Results:** SFDs within the counting areas show two patterns. In most counting areas (13), slopes become increasingly shallow with increasing rock abundance and converge towards each other with increasing size (Figure 1a and 1b), with more rocky SFDs pinching towards their adjacent less rocky SFDs with increasing crater size. Some sites converge more dramatically than others (e.g., Procellarum 58 converges to an overlap, whereas other sites, like Procellarum 53, have SFDs that shallow but do not overlap). The ≥1% and total

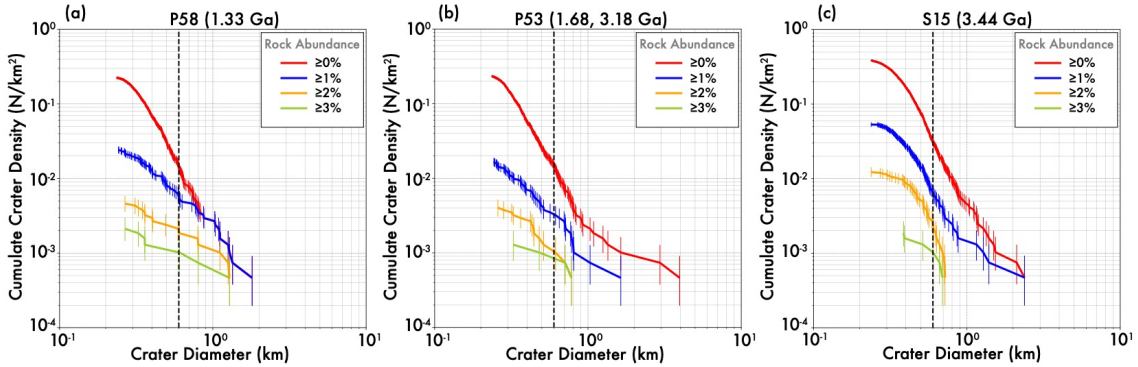


*Figure 1: (a) Converging SFD exhibited by Procellarum 58. The 600 m vertical line is used to mark certainty in crater identification [11]. (b) Shallowing SFD exhibited by Procellarum 53. (c) Parallel SFD exhibited by Serenitatis 15.*

population SFDs for Procellarum 58 fully converge and overlap at ~800 m. As rock abundance increases, large craters with relatively low rock abundance are excluded, and the SFDs no longer overlap. While the converging cases are most common, in a few of the counting areas (2), the SFD slopes are parallel with increasing rockiness (e.g., Figure 1c).

To quantitatively describe the behavior of the SFDs, we calculated their slopes above 600 m. Upon inspection of the SFD slope distribution, we find that the slopes of the total population SFDs are steeper than the ≥1% and ≥2% SFDs (Figure 2).

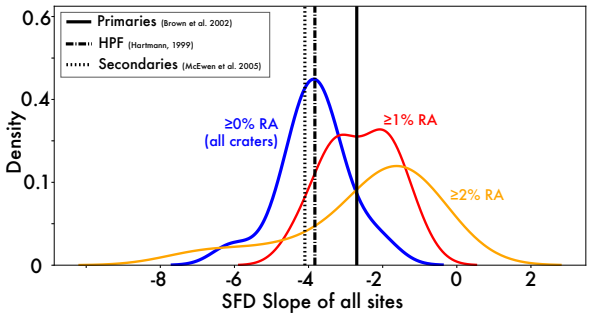


*Figure 2: Smoothed histograms of the ≥0%, ≥1%, and ≥2% SFD slopes for craters >600 m, showing a steeper shift for the ≥0% SFD and a shallowing shift for the ≥1% and ≥2% SFDs. Additionally, the secondary and primary combined SFD slope of -4.1 [15], the primary SFD slope of -2.7 [16], and the Hartmann production function (HPF) [17] slope of -3.82 for craters <1.41 km ([18], equation 1) are shown.*

**Discussion:** The variations in SFD behavior between sites reveal there is a non-uniform process controlling rock excavation. The abundance of small, rocky craters is the major difference between the SFDs of a site exhibiting parallel behavior and a site with converging SFDs. The observed variations are possibly due to mechanical differences in the protolith. A site with a converging SFD may be underlain by a thick, competent protolith, one where smaller impacts may not efficiently eject rocks. In contrast, sites with parallel SFDs may be explained by thin, friable flow types, where rocks fade at the same rate for all crater sizes [19].

Secondary craters may influence rocky crater populations in the converging cases (the parallel cases may be dominated by substrate or lack of secondaries). In Figure 2, the total population SFD slope peak is centered on the HPF slope [17, 18]. The secondary and primary cratering population SFD slope [15] is slightly steeper than the peak of the total population slopes. The peak of the ≥1% SFD slopes shifts towards the primary slope [16], however, the peak is broad. The exclusion of secondaries may not be solely responsible for slope beyond ≥1% SFD slope. The ≥2% SFD slope histogram peaks much shallower than the primary SFD slope, so substrate may play a larger role as rock abundance increases. The convergence of the total population and ≥1% SFDs (e.g., Figure 1a) appears to occur near ~1 km, where the probability that a given crater is a secondary increases [20]. Figure 2 shows that the slopes of most of the total population SFDs are equivalent to the combined secondary and primary impactor population slope [15] and the HPF slope [17, 18] unlike the ≥1% and ≥2% SFD slopes which are more in line with the primary impactor population slope [16].

If secondary impactors are not energetic enough to break up material with high mechanical strength, then secondary craters will have fewer rocks in their ejecta than primary craters. Therefore, if secondaries excavate few blocks, then shallower slopes are expected, as shown by the ≥1% and ≥2% SFD shift towards a primary crater distribution slope (Figure 2).

**Conclusions:** Protolith properties and secondaries are explanations for observed SFD slope variations among mare units. Generally, converging SFDs may be associated with thick, competent flow types, and parallel SFDs may be associated with stacked, thin flows that are possibly more friable. SFD slope analysis suggests that secondary impact craters may be relatively ineffective at excavating rocks and the SFDs of rocky craters may reflect primary cratering populations, as large secondaries are either too ancient to maintain a rocky ejecta population or too weak to eject rocks. Isolating the roles of protolith and secondaries in rock excavation represents future work.

**References:** [1] McKay D. S. et al. (1991). *In Lunar Source-Book*, pp. 285–356., [2] Head J. W. & Wilson L. (2020), Geophys. Res. Letters, 47(20). [3] McEwen A. S. & Bierhaus E. B. (2006). *Annu. Rev. Earth Planet Sci*. 34:533-567., [4] Hiesinger H. et al. (2000). *JGR*. 105, 29239–29275., [5] Hiesinger H. et al. (2003). *JGR*. 108, 5065., [6] Hiesinger H. et al. (2010) *JGR: Planets*. 115(E3)., [7] Barker M. K. et al. (2016), *Icarus*, 273, 46-355., [8] Bandfield J. L. et al. (2011), *JGR*, 116(E12)., [9] Kneissl T. et al. (2011). *Planetary and Space Sci*. 59, 1243–1254., [10] Melosh H. J. (1989). *Impact Cratering*. [11] Robbins S. J. et al. (2014). *Icarus*. 234, 109-131. [12] Tai Udovicic, C. J. (2021) *Craterpy*., [13] Bell S. W. (2020). *samwbell/saturn_counts*., [14] Crater Analysis Techniques Working Group (1979). *Icarus*. 37(2), 467-474., [15] McEwen A. S. et al. (2005). *Icarus.* 176(2), 351-381., [16] Brown P. et al. (2002). *Nature*. 420(6913), 294-296., [17] Hartmann W. K. (1999). *Met. Planet Sci.* 34, 167-177., [18] Neukum G. et al. (2001). *Space Sci. Rev.* 96(1), 55-86., [19] Chertok, M. A. et al. (2022). *LPSC 53*, Abstract #1031. [20] Costello E. S. et al. (2021). *JGR: Planets*. 126(9).